LBL--18728

DE85 006649

# THE HISS SPECTROMETER*

DOUGLAS E. GREINER
Nuclear Science Division
Lawrence Berkeley Laboratory
University of California
Berkeley, CA 94720

Invited talk presented at the
Conference on Instrumentation
for Heavy Ion Nuclear Research,
Oak Ridge, TN, October 22-24,
1984



*This work was supported by the Director, Office of Energy Research, Division of Nuclear Physics of the Office of High Energy and Nuclear Physics of the U.S. Department of Energy under Contract DE-AC03-76SF00098.

# THE HISS SPECTROMETER*

DOUGLAS E. GREINER
Nuclear Science Division
Lawrence Berkeley Laboratory
University of California
Berkeley, CA 94720

This talk describes the Heavy Ion Spectrometer System (HISS) facility at the Lawrence Berkeley Laboratory's Bevalac. Three completed experiments and their results are illustrated. The second half of the talk is a detailed discussion of the response of drift chambers to heavy ions. The limitations of trajectory measurement over a large range in incident particle charge are presented.

## 1. THE HISS FACILITY

The HISS spectrometer is designed to allow multiparticle measurements with good resolution over a large solid angle. The main ingredient is the HISS superconducting dipole that provides up to 6 tesla-meters of bending over a 1 meter gap. Figure 1 shows that the vertical acceptance of the magnet can be as large as 30 degrees for targets placed in the

*This work was supported by the Director, Office of Energy Research, Division of Nuclear Physics of the Office of High Energy and Nuclear Physics of the U.S. Department of Energy under Contract DE-AC03-76SF00098.

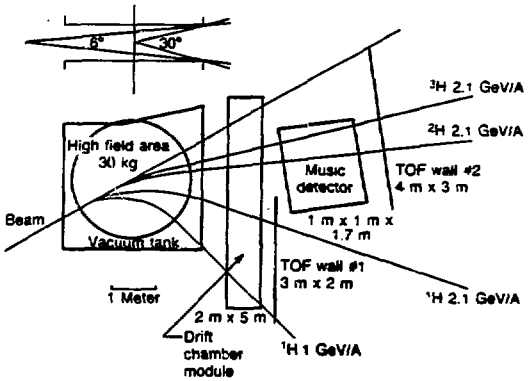


FIGURE 1 HISS Phase II detector system.

center of the dipole. The detector positions are arbitrary. Figure 1 shows a setup that accepts reaction products from infinite rigidity down to 1 GV.

The detectors shown in Fig. 1, with the exception of the drift chamber module, have been built and tested. Hans Sann spoke about the Multiple Sampling Ionization Chamber earlier in the conference, so I will not discuss it further in this talk. There is a high resolution velocity detector, which will be added to the facility, that is not shown. It is based on total reflection of Cerenkov light and will be used for the higher charged particles. Mat Baumgartner will speak about it later in this conference. Experiments to date have used a pair of 1 m x 2 m drift chambers as the tracking device. These chambers were prototypes and will no longer be used. We have done extensive evaluations of a test model of the proposed new, large tracking chamber, and these results will comprise the second half of my talk.

## 2. EXPERIMENTS AT HISS

A list of HISS experiments is shown in Table I. It is clear that there is a large backlog of experiments, including the proposed measurements, which are now approved. In order to show how HISS is used and to give you an understanding of the versatility of the facility, I will show the detector configurations and some of the results of a few of the experiments that have completed data taking.

The first experiment to complete data taking at HISS was experiment 512H, an INS/LBL collaboration led by Shoji Nagamiya. The goal of this experiment was to utilize the large solid angle capability of HISS to measure the high momentum particle spectra at 90 degrees in the center of mass. This experimental configuration is shown in Fig. 2. The A-arm uses the HISS 1 m x 2 m drift chambers and TOF walls along with INS constructed multiwire chambers inside the gap of the magnet. The B-arm was a test of in-field tracking and particle identification for a later experiment. With the field at 1.8 tesla only very energetic particles beyond the nucleon-nucleon kinematic limit would be detected in the A-arm. The resultant proton center-of-mass energy spectrum is shown in Fig. 3. The large solid angle coverage extends the measurements to over three orders of magnitude lower cross sections. It is clear that temperature is a local concept; also, the very large momentum region is not predictable with the conventional cascade calculation. The deuteron and triton spectra are shown in Fig. 4, along with the coalescence-type scaling from the proton spectrum. It is remarkable that this scaling works over 8 orders of magnitude.

TABLE I List of HISS Experiments.

| No. | Title | Institution | Spokesperson | Hours |
|---|---|---|---|---|
| **Approved HISS Experiments** | | | | |
| 512H | Large Pt+multiplicity | INS/LBL | Nagamiya | 150 complete (June 1982) |
| 513H | $^{12}C$ multiparticle | LBL/SSL | Greiner | 138 complete (June 1983) |
| 516H | $^{56}Fe$ multiparticle | LBL/SSL | Lindstrom | 108 |
| 517H | Coulomb decay | LLL/LBL | Berman | 93 complete |
| 521H | p-p correlations | UCLA/LBL | Carroll | 97 (dropped Sept. 1983) |
| 593H | 0 degree pi+z flow | INS/LBL | Hashimoto | 249 complete (Dec. 1983) |
| 614H | Limits of stability | LBL/SSL | Symons | 100 |
| 655H | Missing Gamow-Teller | UCD/LBL | Brady | 48 |
| 662H | Neutron spectra | KSU/LBL | Madey | 262 (May 1984) |
| 683H | $^{16}O$ and $^{56}Fe$ excitation function | LSU/LBL/SSL | Wefel | 96 |
| 684H | pi and k correlations | UCR/LBL | Beavis | 212 |
| 690H | Nuclear radii | INS/LBL | Tanihata | 160 (July 1984) |
| 734H | Exotic nuclei | UCD/LBL | Brady | 42 (18 used) |
| | | | Total | 648 run hours (1026 pending) |
| **Proposed Experiments** | | | | |
| 758H | New nuclear isotopes | UCD/INS | Brady | 120 |
| 761H | Entropy production | MSU/LBL | Westfall | 120 |
| 763H | Velocity Detector Debug | LBL | Olson | 48 |
| | | | Total | 288 |

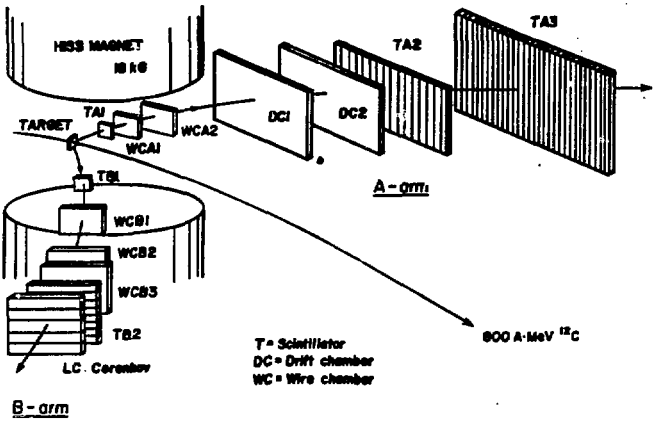


FIGURE 2 Experimental configuration for experiment 512H.

The second experiment involved looking at projectile fragments accompanied by pion production. This INS/LBL experiment 593H used the HISS detectors to observe the projectile fragments and triggered on pions detected by chambers and Cerenkov detectors placed to catch pions bent through 180 degrees by the HISS field (see Fig. 5). It is interesting to speculate, before looking at Fig. 6, as to how much of the original charge of the La still continues in the forward direction. Figure 6 shows the sum of the fragment charges detected in the A-arm when the reaction produces a pi-minus between 50 and 300 MeV/c momentum near 0 degrees. The spectrum peaks at about half the projectile charge, a rather high price to pay to produce a pion. This experiment was also performed on an argon beam. In Fig. 7 we see that the TOF wall has moderate charge resolution through Z=18.

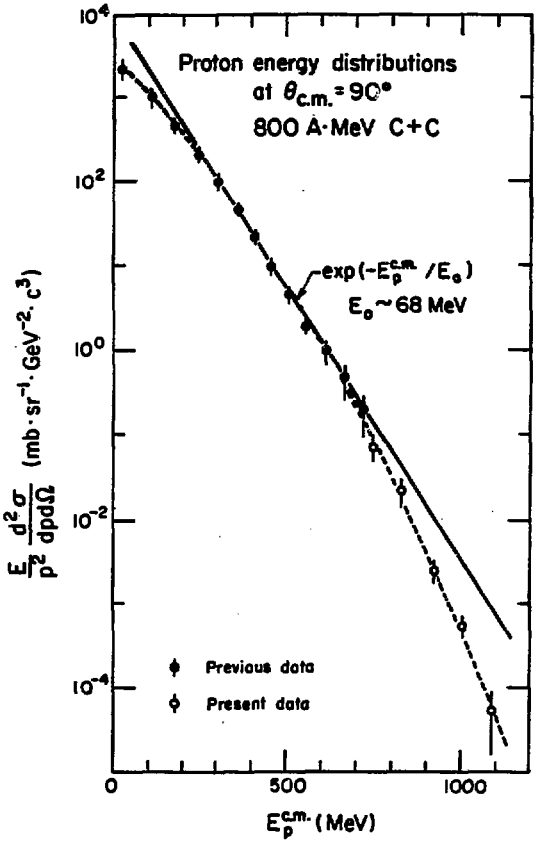


FIGURE 3 Proton center-of-mass spectrum from experiment 512H.

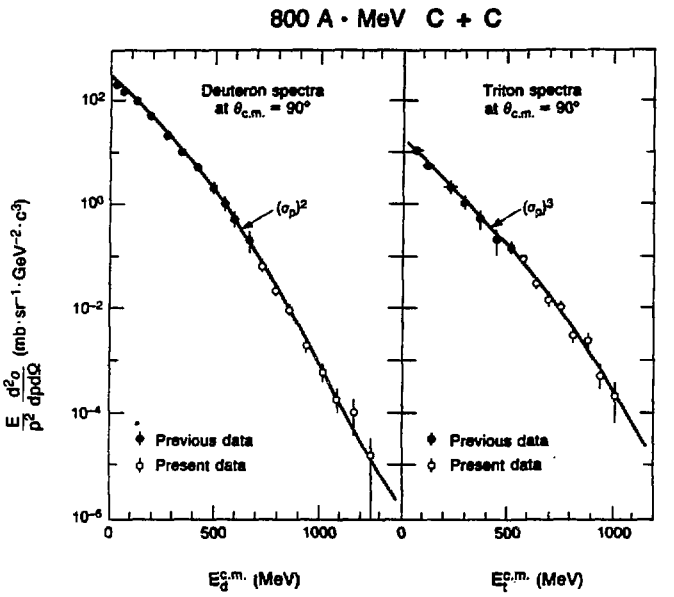


FIGURE 4 Deuteron and triton center-of-mass spectrum from experiment 512H.

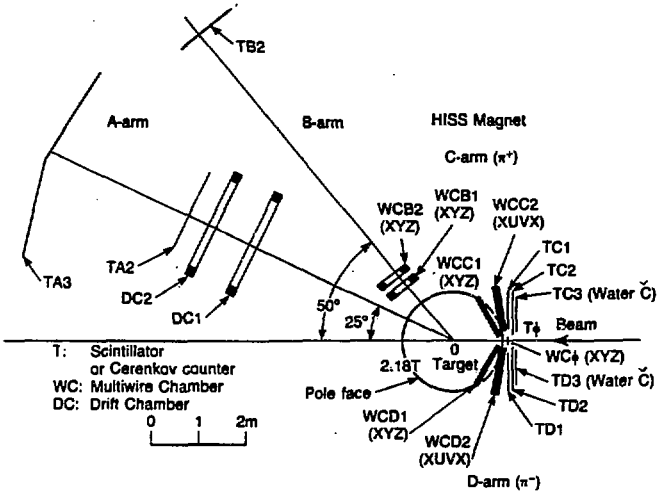


FIGURE 5 Experimental configuration of experiment 593H.

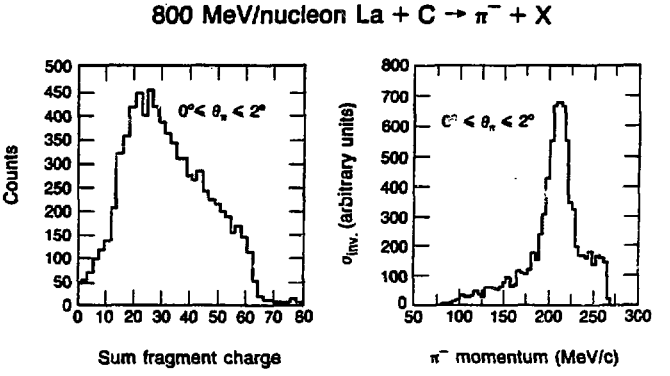


FIGURE 6 Fragment charge sum and pion momentum distributions from experiment 593H.

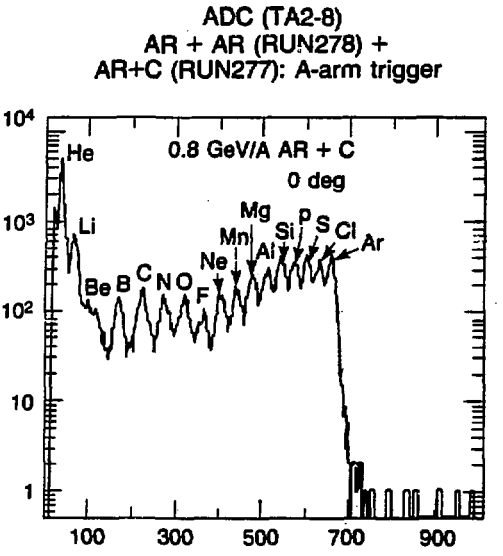


FIGURE 7 Pulse height distribution from TOF wall.

The third experiment (513H) is a HISS group effort designed to shed some light on the reaction mechanism. The basic idea, shown in Fig. 8, is to directly measure the energy transfer in the reaction by detecting all of the projectile fragments allowing reconstruction of the excitation energy these particles have received. The people involved in the experiment are listed in Table II. In Figs. 9 and 10 we see the detector positions, angular acceptance, and rigidity coverage. The drift chambers before the dipole determine the incoming trajectory that allows us to correct for the emittance of the beam. The target is in the center of the magnet; this gives us transverse momentum coverage up to $\pm$400 MeV/c for protons. Fragments are detected by the

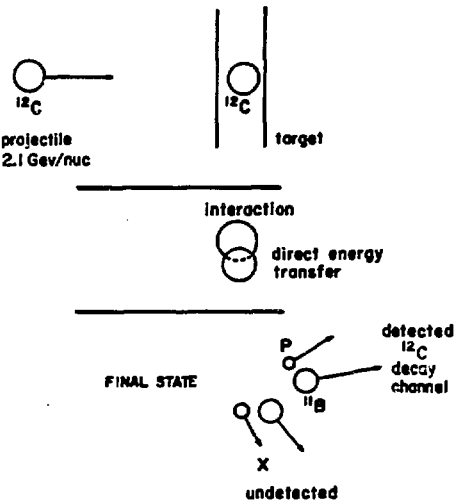


FIGURE 8 Reaction mechanism.

TABLE II Heavy ion spectrometer system group.

| | | | | | |
|---|---|---|---|---|---|
| M. Baumgartner | LBL | J. Engelage | UCLA | D. Olson | LBL |
| E. Beleal | LBL | I. Flores | UC/SSL | J. Porter | LBL |
| F. Bieser | LBL | D. Greiner | LBL | H. Sann | GSI |
| M. Bronson | LBL | P. Lindstrom | LBL | T.J.M. Symons | LBL |
| H. Crawford | UC/SSL | C. McParland | LBL | R. Wada | GSI |

THE HISS SPECTROMETER

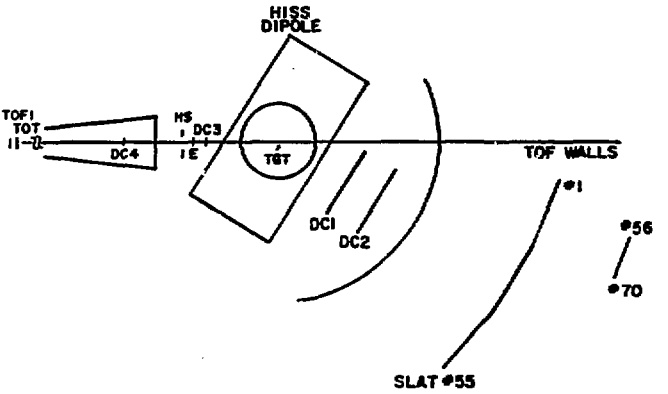


FIGURE 9 Experimental configuration of experiment 513H.

drift chambers and TOF walls, with a second wall for redundancy in the high flux region near Z/A = 0.5. Triggering requires a good beam trajectory, Z=6 incoming and no Z=6 coming out, determined by a small scintillator placed near the TOF wall in the position of the beam focus. The relative positions of the various projectile fragment peaks in rigidity space are shown in Fig. 11. The desire to see $^{1}H$ and $^{3}H$ in the same event determines the lateral extent of the desired coverage. Performance of the TOF wall as a charge sensitive detector is shown in Fig. 12; charge resolution is about 0.2e. The single plane resolution of the drift chambers is shown in Fig. 13.

The proton spectrum is quite broad. In Fig. 14a,b we plot the hit positions of $^{1}H$ and $^{3}H$ for events containing at least one proton and one triton. It is clear that the proton distribution is quite broad, and we could even use more coverage. It is interesting to look at the invariant

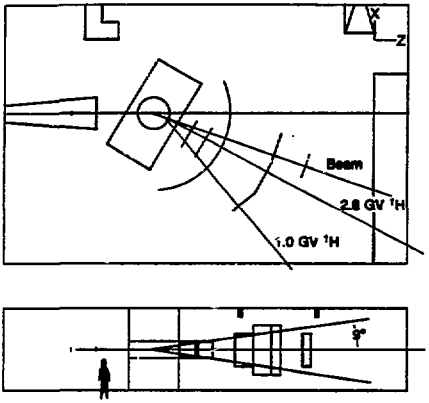


FIGURE 10 Rigidity limits for experiment 513H.

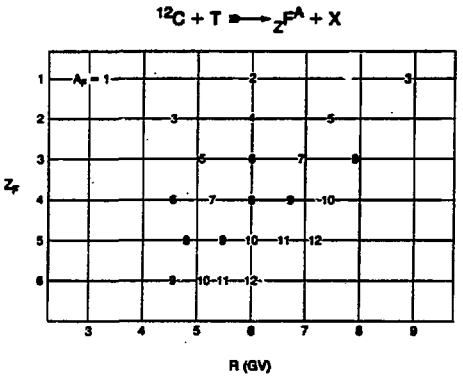


FIGURE 11 Central rigidities of secondary fragments.

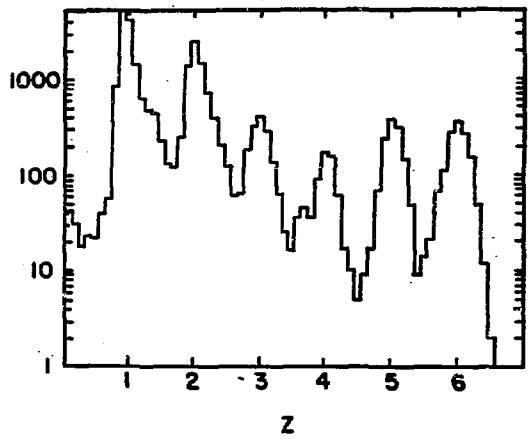


FIGURE 12 Charge distribution from TOF wall.

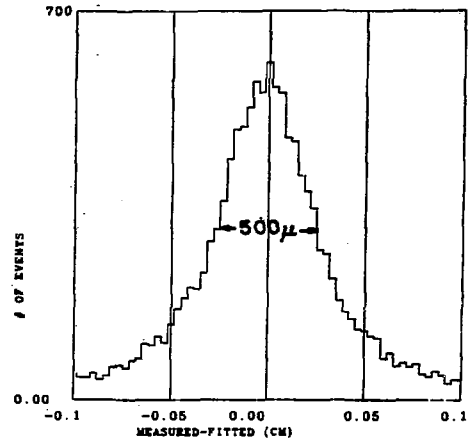


FIGURE 13 Single plane position resolution (Z=6).

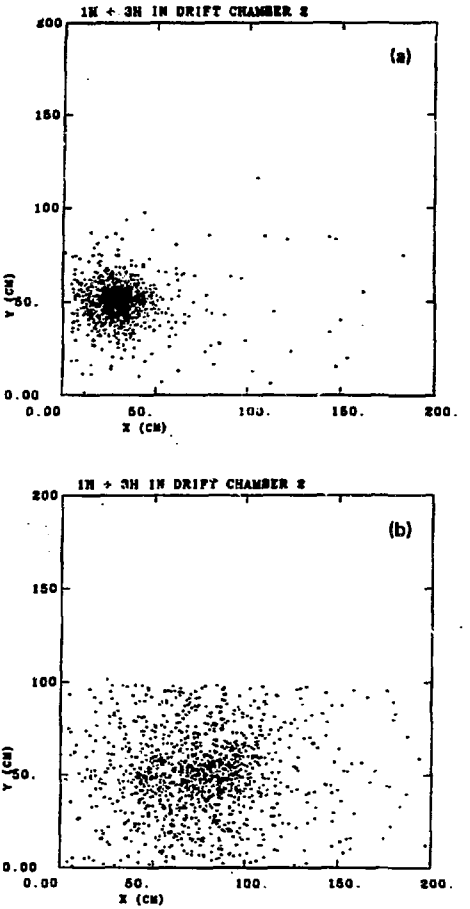


FIGURE 14 Hit pattern: (a) tritons and (b) protons.

mass of this particle pair in Fig. 15. One sees the expected peak at the mass sum due to the many events where the proton and triton come out at low relative momentum along with a long tail of several hundred MeV where possible bound states can show up. We would expect to see bound state effects in the corresponding plot for events containing two helium products (Fig. 16). Here we have a very much finer energy scale and hints of structure presumably produced by $^{8}$Be bound states. These examples represent a first analysis of 1% of the available data.

## 3. TRACKING CHAMBERS FOR HEAVY IONS

We turn now to the technical problem of determining the trajectories of heavy ions at relativistic energies. To demonstrate the effects of the copious delta ray production

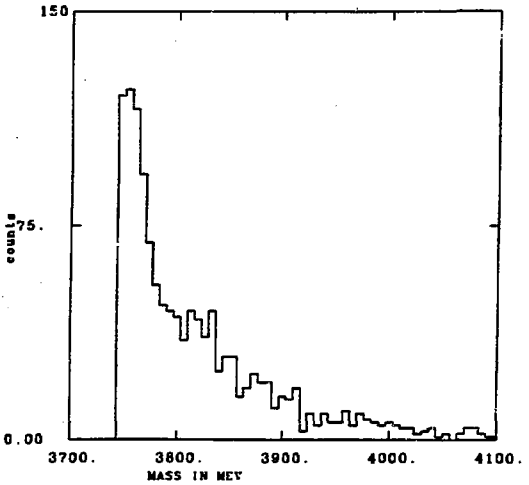


FIGURE 15 Proton plus triton invariant mass.

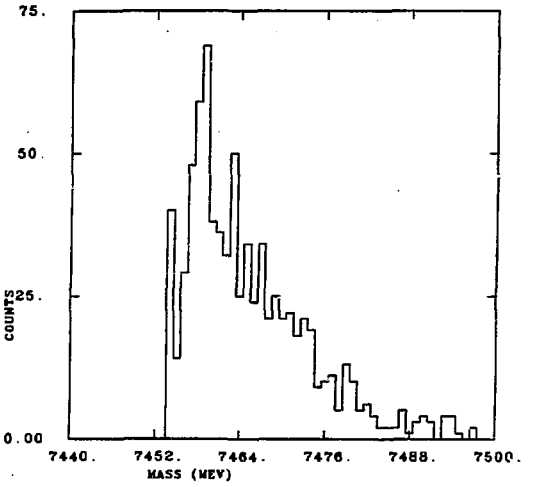


FIGURE 16 Two alpha invariant mass.

at these energies I show in Fig. 17 a photograph, taken by the Riverside group, of 1.4 GeV/nucleon La in the steamer chamber with the magnetic field turned off. The spatial extent of the delta ray cloud is quite large, and if one is interested in detecting low and high charge particles simultaneously the fact that delta rays are charge-one particles cannot be neglected. This problem is a major one for the field and has been the object of considerable study by the HISS group. The goal of our study was to develop and demonstrate a design to satisfy the requirements listed in Table III. This year Fred Bieser and Toshio Koybayshi have conducted extensive tests of our proposed solution outlined in Table IV. The 12-plane test chamber is schematically shown in Fig. 18. The design uses multiple measurements in the

FIGURE 17 Lanthanum streamer chamber event.

S,T,U directions to achieve sufficient redundancy to identify multiple tracks. The drift cell configuration is designed to allow variation of the gain, keeping the drift field relatively constant (Fig. 19). The ground planes between the twelve modules capture the electrons produced outside of the sense planes and isolate the drift fields from one another. The variation of drift field when the gain is changed by 400 volts is shown in Fig. 20. We see a rather small variation allowing drift time calibrations to be relatively independent of operating voltage.

In Fig. 21 we have plotted the efficiency curves for the drift chamber obtained for the Z=1,5 beams. The Z=1 case shows the standard behavior: the chamber is plateaued at 100% efficiency and the single hit efficiency is almost 100% indicating that the chamber gives one hit per incident particle. As we increase the incident beam charge we see

**TABLE III** Requirements for a drift chamber for high energy heavy ions.

---

**GENERAL REQUIREMENTS**

- Good angular resolution

$$\frac{\Delta A}{A} = \sqrt{\left(\frac{\Delta R}{R}\right)^2 + \left(\frac{\Delta Z}{Z}\right)^2 + \left(\gamma^2 \frac{\Delta\beta}{\beta}\right)^2} \sim 0.2\% \text{ at } A = 100$$

- Good double track pair resolution

**REQUIREMENTS UNIQUE TO HIGH ENERGY HEAVY IONS**

- Large dynamic range

  i.e. $1 \leq Z \leq 92$ at $0.5 \sim 2.0$ GeV/nucleon

  Energy loss $(\alpha Z^2) = 1$ to $\sim 9000$ for Z=1 to 92

- $\delta$-ray rejection + full efficiency for Z=1

  No. $\delta$-rays $\alpha$ $Z^2$

  $\delta$-rays are minimum ionizing particles!

- Thin chamber

  due to { large reaction cross section; large energy loss ($\alpha$ $Z^2$) }

---

TABLE IV Solutions.

**TECHNIQUES**

- Constant Fraction Discriminator (CFD)
  - — to pick up the timing signal of core ionization in the presence of $\delta$-rays
  - — chamber is still sensitive to $\delta$-rays
- Pulse height information from every wire
  - — to find the cell hit by the heavy ion
  - — to reject spurious hits from $\delta$-rays
- Thin chamber
  - — single gas volume
- Distributed planes
  - — simpler track finding
- Good mechanical rigidity + good positioning
  - — $\delta_{position} \sim 40\mu$ for all wires

**STRUCTURE + ELECTRONICS**

- Cell structure
  - — 1 cm drift length with field shaping
- 12 planes : S T U S'T'U' S'T'U' S T U
  - — 0°, ± 60°, 10 cm apart
- Modular plane on a thick base plate
  - — Aluminum stiffner
  - — $\delta_{position} \sim 40\mu$ from known line for all wires
  - — Single gas volume : 40 (H) × 30 (V) × 120 (L) $cm^3$
- P-10 gas : Ar 90% + $CH_4$ 10%
- Single hit TDC (limited by CFD)
- Current integrating ADC

**TEST BEAMS**

- Energy: ~1 GeV/nucleon
- Beams: H (Z=1), He (Z=2), Li (Z=3)
  Be (Z=4), B (Z=5), Ne (Z=10)
  Fe (Z=26), Xe (Z=54), U (Z=92)

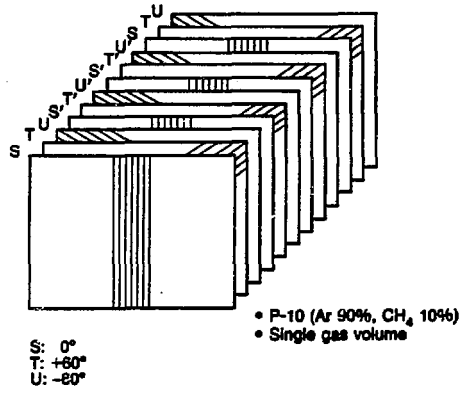


FIGURE 18 Schematic view of prototype drift chamber.

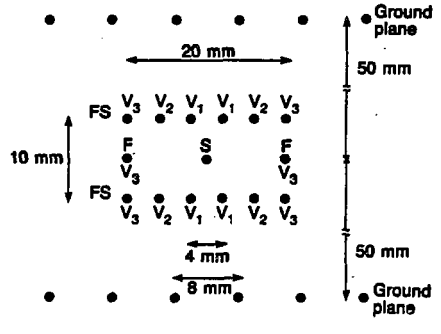


FIGURE 19 Cell geometry.

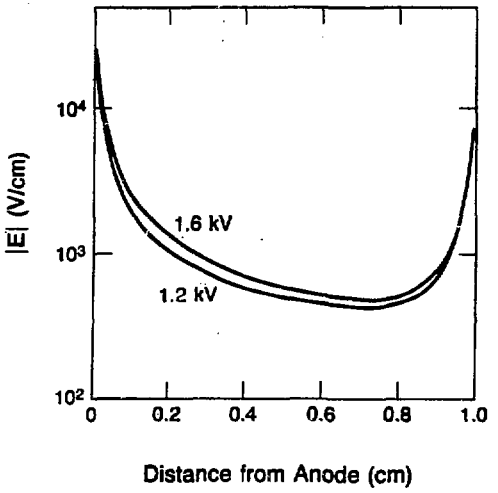


FIGURE 20 Electric field in midplane.

that the voltage at plateau decreases as expected due to the larger de/dx. However, the single hit efficiency drops off, and the higher charge cases never reach 100%. This is due to delta rays at large angles to the track depositing sufficient energy to trigger other wires in the chamber. It is clear that a chamber that is running at 1.5 kV in order to see protons will see single hits for a boron track only 50% of the time.

The fact that the single hit efficiency does not reach 100% means that in the region around Z=5 the delta rays can deposit as much energy as the primary track in a given cell. At higher charges this effect decreases and it again becomes possible to achieve 100% single hit efficiency over a very limited range of incident charge. These data alone tell us

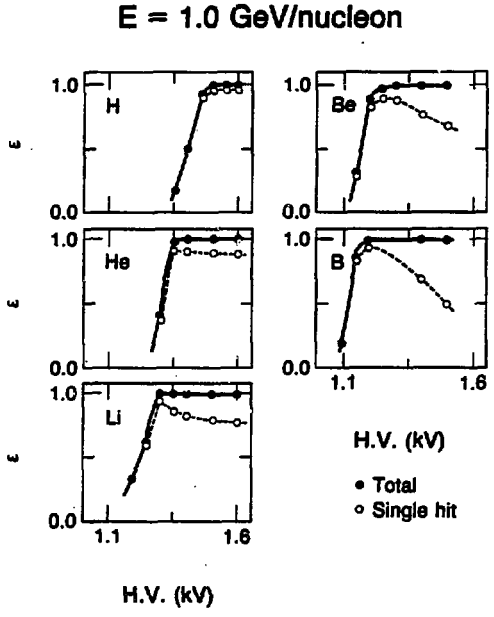


FIGURE 21 Efficiency curves for charges 1-5.

that in the drift chamber, with its constant fraction front end, the worst case for suppressing delta ray triggers in a single cell will be in the region of incident particle charges of Z=5.

In what follows I limit myself to discussing the response of a single plane of the drift chamber. The average number of hits per plane as a function of incident charge and voltage is shown in Fig. 22. The qualitative result from the earlier streamer chamber photograph is seen with a vengeance. The total number of wires in a plane is 20,

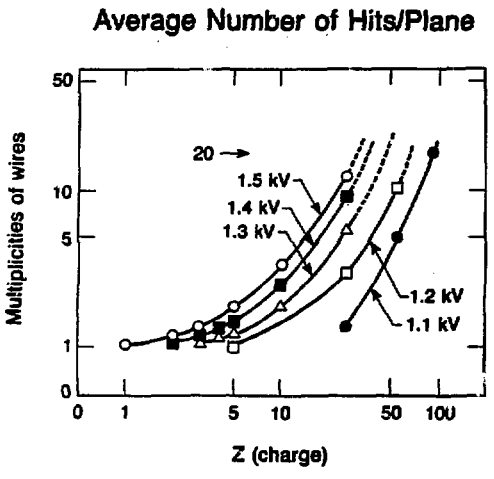


FIGURE 22 Multiplicity as a function of charge.

covering a distance of 20 cm on each side of the primary particle. Examination of these data makes it clear that there is no operating voltage covering a large variety of charges with single hit response. For the higher charges every wire in the chamber gives a signal regardless of the gain.

So TDC information is not enough; we need to examine the charge deposited as a function of position. Figure 23 shows the pulse height spectra as a function of cell number for Fe,Xe and U projectiles. As we hoped the cell with the heavy ion is clearly separated over this wide charge range by the ADC information. An interesting fact is that the distribution of energy around the track is not the same

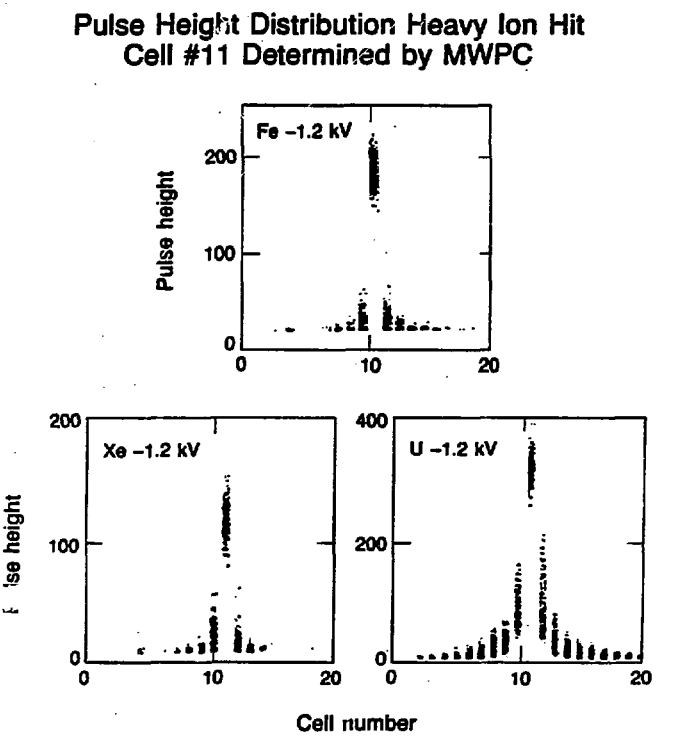


FIGURE 23 Pulse height distributions vs. cell number.

shape for the different incident particles. We have not calculated this yet, but feel that it is connected with the multiple scattering of the delta rays.

Figure 24 demonstrates the selection of the proper drift cell by choosing the largest pulse height in each plane. The plots for incident particles Fe, Xe, and U are arranged in sets of each S,T,U combination and show on the

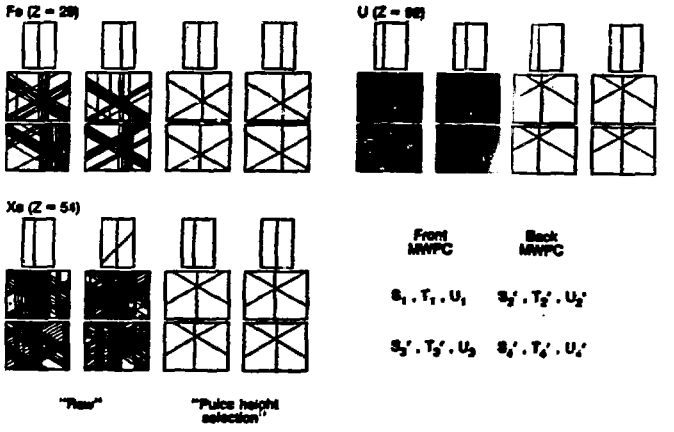


FIGURE 24 Typical wire patterns at H.V. = -1.2 kV.

left the uncut data and the ADC-selected wires on the right. Thus for a single chamber voltage of 1.2 kV we can use the ADC information to locate the proper cell; later we will see the accuracy of the TDC information within the selected cell.

At this point I would like to discuss the energy deposition in a little more detail. To illustrate the distribution of the central core ionization we plot in the upper half of Fig. 25 the distribution of pulse heights for all wires in a plane for a set of Xe events. In the lower half of Fig. 25 we see the "selected" and "rejected" spectra. The selection criterion was to take the largest pulse height seen in the entire plane. This gives the energy deposited in a two-centimeter-wide interval about the track. The rejected spectrum is what is left. Because these two spectra overlap, an absolute cut in pulse height will not always

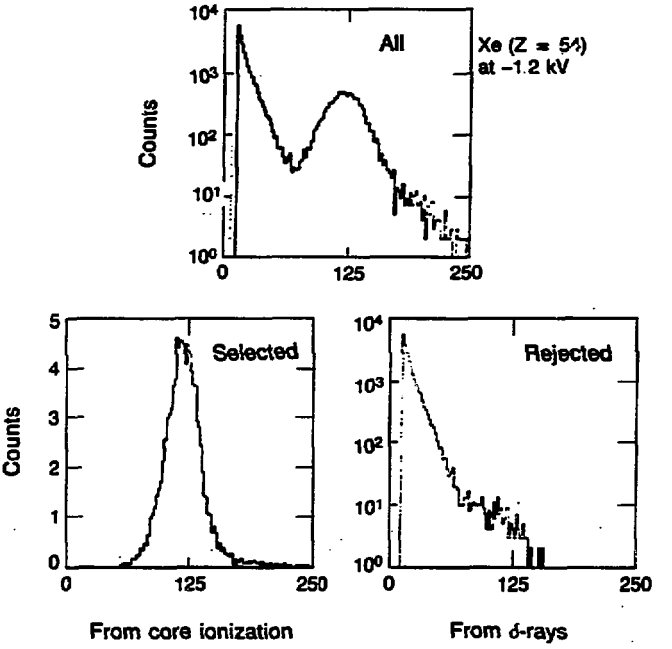


FIGURE 25 Single wire pulse height distributions.

select the correct cell due to the variations in both energy loss and possible variations of response depending on track position within a cell. Note that the pulse height information summed over the 12 planes available gives a rough charge estimate. This information should prove useful in trajectory reconstruction in conjunction with other more

sensitive but less segmented charge detectors. In Fig. 26 we see the pulse height from the two-centimeter region about the track varies as the 1.5 power of the charge. This quantifies the shape change mentioned earlier. As the charge of the projectile increases we see that more of the energy is deposited at greater distances from the trajectory. Also for charges somewhere between 10 and 26 the spectrum of energy deposited in this region becomes gaussian. As a consistency check we sum all the energy seen in one plane in

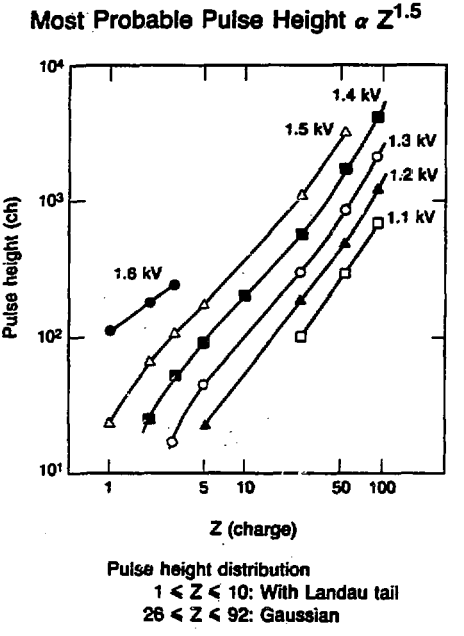


FIGURE 26 Most probable pulse height of one wire vs. particle charge.

Fig. 27. The Z-squared dependence is recovered along with the correct Landau shape for all charges.

Using the trajectory as determined by the multiwire we can examine the spatial linearity and resolution of the drift chamber. Figure 28 shows the TDC response of the drift chamber for charges ranging from 5 to 92 recorded at the same chamber voltage. Some nonlinearity near the anodes develops for the lower charges. We believe this is due to changes in the pulse shape from the radical change in the distribution of electron arrival time at the anode, and it indicates that calibrations will change slightly as a function of charge. The chamber resolution for tracks 0.5 cm

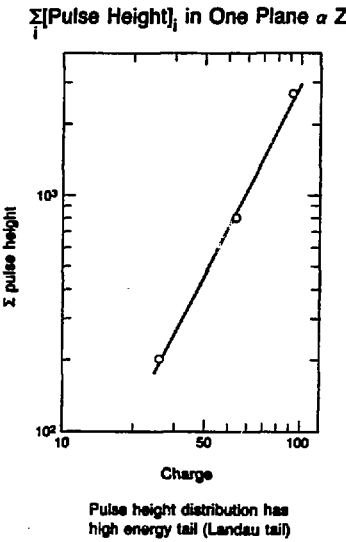


FIGURE 27 Sum of pulse heights from all wires in a plane.

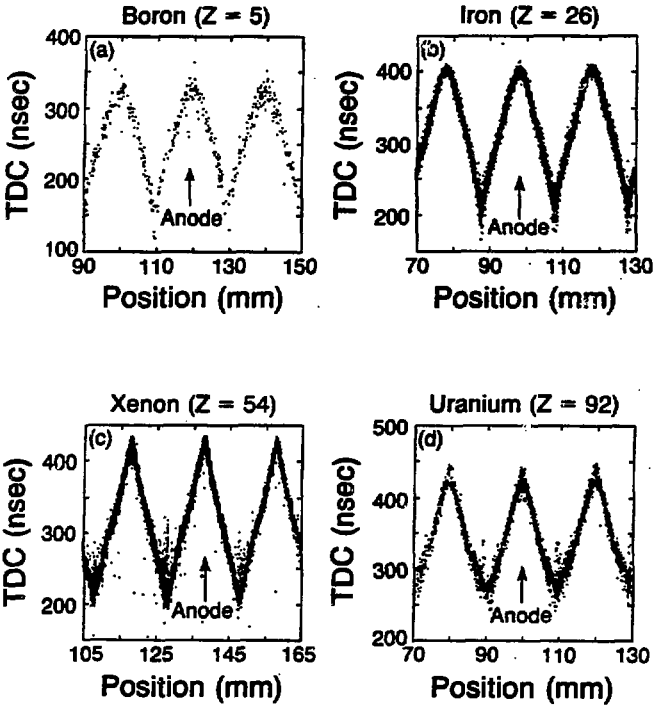


FIGURE 28 Space-time relation for various charges.

from the anode is shown as a function of chamber voltage and particle charge in Fig. 29. The optimum operating voltage varies with charge so that the dynamic range and accuracy requirements of the experiment must be considered when determining the running voltages. The plotted resolutions are a slight overestimate because the trajectory uncertainty of the MWPC's is not removed.

Another concern is particle pair separation. If there are other tracks near a heavily ionizing trajectory, the delta ray cloud can mask their signals. This cylinder of confusion is most probably a basic limitation of gaseous trajectory measurement devices applied to heavy ions. To see the possible magnitude of this limitation we use the pulse height information to show the minimum detectable charge as a function of distance from primary tracks of Fe,

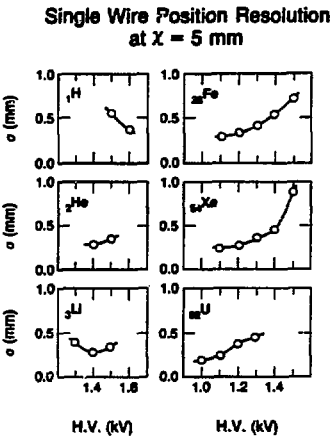


FIGURE 29 Single wire position resolution for various charges.

Xe, and U (Fig. 30). Some improvement may be made using peak sensing ADC's, utilizing redundancy and magnetic fields, but we don't expect too much.

The results presented here will form the basis for our design of the large area tracking chamber at HISS. These results and conclusions are summarized in Table V.

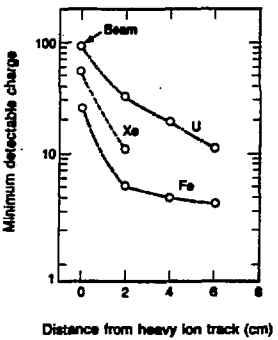


FIGURE 30 Estimate of double track pair resolution from pulse height information.

TABLE V Bevalac test results.

**RESULTS**

1. Efficiency
   - ~100%
2. Pulse Height Information
   - reject $\delta$-ray signals, ~ 100%
   - visible energy loss in one cell, $\propto Z^{1.5}$
   - total energy loss ($\Sigma$ pulse height), $\propto Z^2$
   - shape
     $1 \leq Z \leq 10$: asymmetric + Landau tail
     $26 \leq Z \leq 92$: symmetric (Gaussian)
3. Position Resolution + Time-Distance Relation
   - Multiple scattering limit at the optimum voltage for each charge
   - Parameterization of time-distance relation as a function of charge at a given voltage for actual experiment required
4. Double Track Pair Resolution
   - estimate from pulse height distribution
   - real 2 track finding algorithm being developed
5. Charge Resolution or Energy Loss Resolution
   - Using 12 sampling
     $26 \leq Z \leq 92$ : averaging $\sigma_z \sim 0.8$
     $1 \leq Z \leq 10$ : truncated mean

**CONCLUSIONS**

1. Limited Dynamic Range
   - Requiring ~ 300 $\mu$ resolution

| High Voltage | Range |
|---|---|
| −1.8 kV | $1 \leq Z \leq 12$ |
| −1.4 kV | $2 \leq Z \leq 26$ |
| −1.2 kV | $5 \leq Z \leq 92$ |
| −1.1 kV | $8 \leq Z \leq 92$ |

2. Double Track Pair Resolution
   - Detection of Z=1 possible outside ± 20 cm from uranium track (worst case)

This report was done with support from the Department of Energy. Any conclusions or opinions expressed in this report represent solely those of the author(s) and not necessarily those of The Regents of the University of California, the Lawrence Berkeley Laboratory or the Department of Energy.

Reference to a company or product name does not imply approval or recommendation of the product by the University of California or the U.S. Department of Energy to the exclusion of others that may be suitable.